

Comparative study between the structural and tectonic situation of the Southern Sinai and the Red Sea, Egypt, as deduced from magnetic, gravity and seismic data

Mohamed EL-BOHOTY¹, Ladislav BRIMICH², Ahmed SALEH¹,
Salah SALEH¹

¹ National Research Institute of Astronomy and Geophysics (NRIAG), Egypt
e-mail: elbohoty3@gmail.com, salahsmm@yahoo.com

² Geophysical Institute of the Slovak Academy of Sciences
Dúbravská cesta 9, 845 28 Bratislava, Slovak Republic, e-mail: geofbrim@savba.sk

Abstract: The present study is concerned with the analysis of magnetic gravity and seismic data for the regions of the South Sinai and the Red Sea areas aiming to evaluate the subsurface geologic active structures. The magnetic method of prospecting gives an effective presentation of the subsurface structures. Moreover, the wavenumber filtering is carried out utilizing three types of filters with varying wavelengths. The application of these tools on the magnetic and gravity data discriminated the variable sources of specific depth ranges for the residual and regional anomalies, as well as those limited to a certain depth interval. Also it was found that the main tectonic trends have taken the NE–SW and NW–SE directions. A three-dimensional (3D) interpretation of the Bouguer anomaly and aeromagnetic maps of the Gulf of Suez rift and the northern part of the Red Sea rift are presented. A high-resolution 3D model constrained with the seismic results reveals a possible crustal thickness and density distribution of the north Red Sea rift between the sedimentary cover and the mantle.

Key words: geomagnetic measurements, interpretation of the gravimetric measurements, filtering, the Southern Sinai, the Red Sea

1. Introduction

The study of the structural and tectonic situation of the Red Sea and the Southern Sinai area is very important in order to determine the structural and tectonic setting of the subsurface areas and its geodynamics. The structure of the area has become significant as the basement and its fraction

played the main role in the seismic activity. The filtering technique was used to separate the anomalies of different wavelengths from each other. This technique was applied to the RTP aeromagnetic maps and gravity map, to extract the potential signal. The filters technique was used in the Red Sea and the Southern Sinai areas to determine the subsurface structures at different depths and to calculate the depth at which deformation occurs.

Geophysical methods have been applied to gravity and magnetic data to perform the 3D forward gravity and magnetic modeling developed by *Schmidt and Götze (1998)*. The depth of the upper part of the Earth's crust will be investigated in addition to the depth of the Moho. Many studies have discussed the evolution of the Red Sea rift as a key to the understanding of continental rifting and the initiation of sea floor spreading (*Drake and Girdler, 1964; Tramontini and Davies, 1969; Makris et al., 1983; and Gaulier et al., 1988*). The results obtained from a high-resolution 3D gravity and magnetic models fill the gap between Gulf of Suez rift and Sinai in the north and the Egyptian part of the north of the Red Sea region in the south. In general, the present investigation is mainly concerned with the study of the major crustal structures of the north of the Red Sea and Gulf of Suez rift using different approaches to gravity and magnetic data interpretation.

2. Geological settings

The studied area is divided into two parts: the first, located along the Red Sea between latitudes $26^{\circ} 20' - 28^{\circ} 22' \text{ N}$ and longitudes $33^{\circ} 46' - 34^{\circ} 30' \text{ E}$, (Fig. 1), and the second area is located in the southern part of Sinai, between latitudes $28^{\circ} 00' - 29^{\circ} 00' \text{ N}$ and longitudes $33^{\circ} 00' - 34^{\circ} 30' \text{ E}$ (Fig. 2). The Red sea forms an elongated, northwest striking depression with a length of approximately 2000 km separating the African plate from the Arabian plate. Its northern part represents a continental rift in its final stage and close to the following stage of the sea floor spreading whereas the southern part exhibits an already organized sea floor spreading, since 5 M ago (*Rosser, 1975*).

The Southern Sinai lies between the eastern and western flanks of the Red

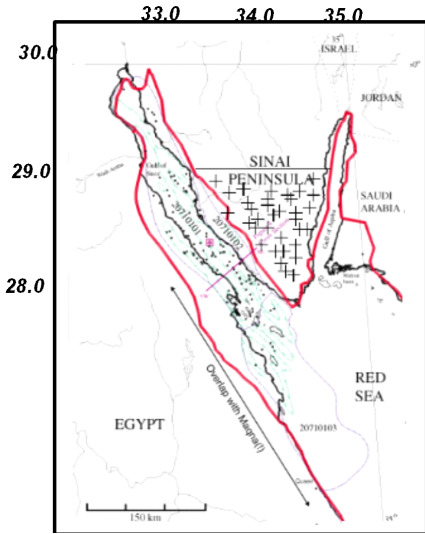


Fig. 1. Location map of the Southern Sinai area.

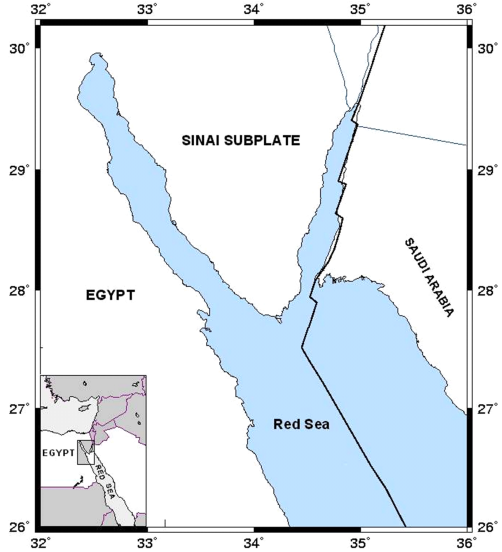


Fig. 2. Location map of the Red Sea area.

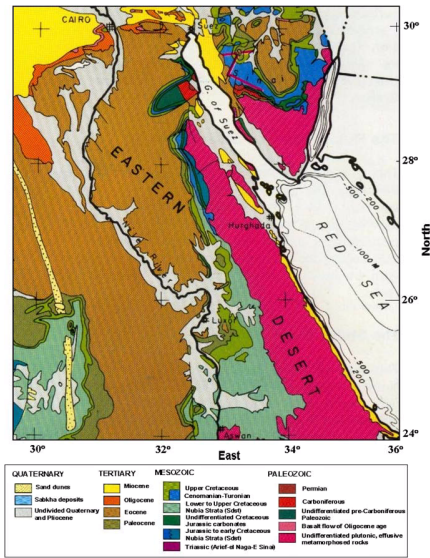


Fig. 3. Surface geological map for the study region (from *Egyptian Geological Survey, 1994*).

Sea Gulf rifts (Fig. 3) and it has been subject to intensive faulting during the rift activities. There are two main fault structures, the first one runs along the contact between the sedimentary section and the basement complex, while the second one runs along the Gulf of Suez coast to the west. These two main faults are dissected comparatively by minor transversal faults and sometimes they branch to a series of small and roughly parallel step faults (*Abdallah and Abu Khadra, 1976*). The Red Sea Basin Province originated as an Oligocene continental rift impacted by left-lateral wrenching. Rift location and borders are defined by crustal weaknesses created more than 500 Ma, including the late Proterozoic to early Paleozoic cratonization of the Arabian-Nubian shield, its suturing to the African continent, and subsequent supercontinent breakup. Those events resulted in the juxtaposition of structurally and compositionally different basement terranes. *Said (1962)*, and *El-Gezery and Marzouk (1974)* showed that the depth of the basement increases northwards towards the Mediterranean Sea. The Paleozoic rocks are characterized by continental clastic deposits. The marine episodes are minor in space and time.

The Paleozoic period ends with the Upper Carboniferous Lower Permian marine deposition, that followed the Hercynian orogenic phase and the subsequent erosional period. Predominant continental deposition started again in the Mesozoic. The Cenozoic witnessed the transformation of the Tethys into the Mediterranean Sea during the Paleocene-Eocene. The Miocene was a period leading to the formation of present Red Sea coast sediments and sediments in the northwestern part of the Gulf of Suez. The Quaternary was determined by regression with minor transgression. Uplift and tectonic disturbances mark the Pliocene-Quaternary boundary in the Red Sea region. Volcanism occurred in the Red Sea axial trough (*Said, 1990*).

3. Gravity, magnetic and seismic data

A considerable amount of gravity data is now available to unravel the gross crustal structure of the Red Sea region. The present work utilizes the Bouguer gravity data of the *General Petroleum Company (GPC), 1980* Cairo, Egypt, which published the set of Bouguer maps of Egypt on 1:500 000 scale by compiling all available data. Gravity data values were obtained at

1 min intervals with discrepancies at ship track intersections of less than about 1 mGal for the northern sections and not more than about 3 mGal in the worst cases. The aeromagnetic map of the Red Sea was prepared by the EGPC (*General Petroleum Corporation, 1990*) with a flight elevation of 1 km. As for the aeromagnetic map of the South Sinai region, it has been prepared by the Egyptian Geological Survey in 2001 and then presented published by Ismail in the scientific conference held in Tanta University in 2001 (*Ismail et al., 2001*). The aeromagnetic data was digitized into computer using *Geosoft program (2008)*. Processing of the available aeromagnetic data was carried out using Geosoft mapping and Processing system. Reductions to the north magnetic pole were applied to the total intensity aeromagnetic map of the South Sinai area (Fig. 4) to remove undesired distortion of the magnetic anomalies due to the effects of the inclination of the geomagnetic field. Comparison of the two maps (Figs. 4 and 5) shows the shifting of the RTP magnetic anomalies to the north direction relative to their positions in the total magnetic intensity map in addition to small change in their shapes. Earthquake data used in this study cover the time interval from 1906 to 2003. A great numbers of events with magnitude range from unassigned to 6.9 were reported for both Red Sea and South Sinai (Fig. 23).

3.1. Description and structural indications of the aeromagnetic anomaly maps

The detailed analysis of the RTP aeromagnetic map for the South Sinai area (Fig. 5) shows strong positive anomalies concentrated in three key areas. The first area is located on the west side, with a positive magnetic anomaly axis of high values taking the northeast-southwest direction. The second area of the strong positive magnetic anomalies is located in the middle of the region and consists of one closure irregular in shape and small in size. The last area of the high magnetic anomalies is located in the southeastern part and extends to the edge of the south-east. The strong magnetic anomalies may be attributed to the occurrence of subsurface basic intrusions of high magnetic content. The central part is characterized by intensive negative anomaly constituting several peaks. These peaks reflect high magnetic susceptibility amplitudes. These anomalies may be inter-

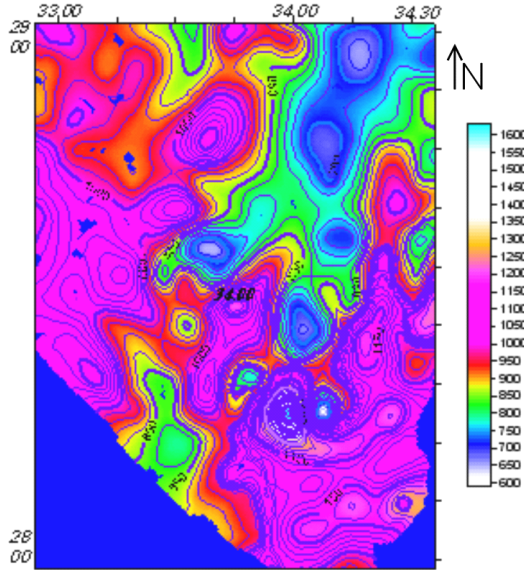


Fig. 4. Aeromagnetic map of the Southern Sinai area.

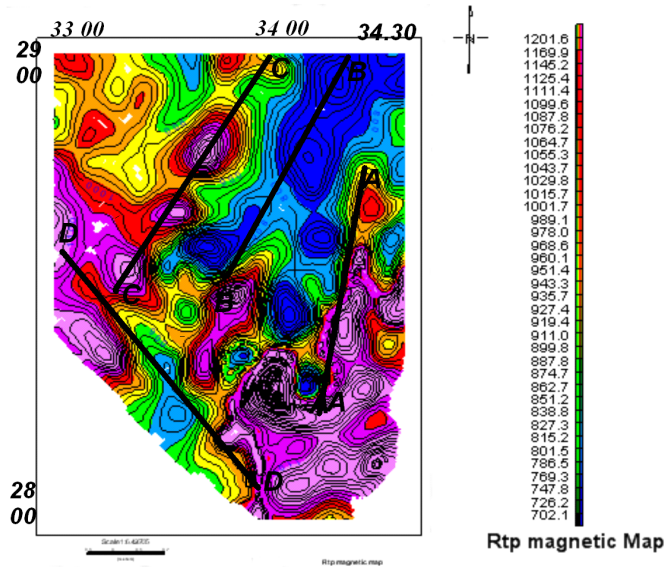


Fig. 5. RTP aeromagnetic anomaly map of the Southern Sinai area. The lines A, B, C and D denote the location of the magnetic anomaly trends reflecting the presence of dislocation in the basement surface.

preted as structural low or low-down-faulted basement blocks. This main magnetically high area is separated from adjacent low area by steep magnetic gradient with a shallow basement rock. This steep gradient indicates that the area is structurally controlled by a fault having a major axis in NE–SW direction.

Magnetic structures

The study of the structural anomaly trends of the Southern Sinai area as well as the regional magnetic trends which have been delineated in Fig. 5, indicates that, there are at least 4 essential structural – morphological elements, mostly reflecting the presence of dislocation in the basement surface that correlate well with the regional magnetic trends. It should be stated that magnetic structures do not occur at random but are generally aligned along definite and preferred axes forming trend that can be used to define magnetic bodies. These can be grouped in a system having a different direction as follows:

1. High magnetic anomaly trend (A–A)

This trend occupies the eastern part of the study area by anomaly of irregular shape with positive polarity, considerable relief trending N 15 E in the vicinity of the studied map. This high trend is separated from the next low trend by an intensive magnetic gradient probably expressing a normal fault.

2. Low magnetic anomaly trend (B–B)

This trend is following the above mentioned high to the west in the form of three anomalies of considerable relief and high gradient. These anomalies have circular shape, negative polarity, low frequency and N 15–25 E trending. The anomalies along this trend can be interpreted as a result of shallow sedimentary basin.

3. Low magnetic anomaly trend (C–C)

This trend of magnetic low stretches the central part of the study area as irregular anomaly of low frequency, negative polarity and mostly NE–S trending.

4. Low magnetic anomaly trend (D–D)

This trend of low magnetic anomalies is located in the southwestern

corner of the study area and is composed of anomalies of low frequency, irregular shape, high gradient and NW–SE trending. These anomalies are thought to be a result of the increase of acidity in the rocks forming the basement complex.

The RTP aeromagnetic anomaly map of the Red Sea area (Fig. 6), reveals that the map includes a wide elongated positive anomaly occupying the major part of the map and having NW–SE trending. It follows towards the Southern side by four closures of negative anomalies contour, values ranging between +100 nT and –100 nT and also has NW–SE trending. In part that is located in the far northwest of the Red Sea coast, the anomaly is considered the strongest positive magnetic anomaly in the Red Sea area as a whole. Such magnetic anomaly is suggested to be associated with source rocks of a basic nature. The observed relative difference in amplitude of the magnetic anomalies recorded over this part may be related to either their lateral variation in topographic relief. The elongated anomaly zones with steep gradient indicate considerable subsurface faulting with NW–SE trending. These anomalies can be explained as a result of magnetic basaltic extrusions associated with the NW–SE faulting trend. The map shows also local magnetic anomalies superimposed on the regional magnetic field. These anomalies are most probably related to basement faulting structure.

3.2. Description and structural indications of the Bouguer anomaly map

The Bouguer anomaly map of the Red Sea area (Fig. 7) exhibits a positive linear anomaly along the eastern and western shoulders of the Red Sea rift with sharp gradient extending NW–SE. The negative values are in accordance at northern and south western parts of the area with the general gravity trend N 30E and N 30W. The anomaly increases in magnitude with a decrease in the relief of the topography and attains its maximum of +95 mGal along the axis of the Red Sea rift floor. This map can be divided into a number of distinct areas based on anomaly size, trend and gradient, which can be related to regional geology. A belt of the first, second and third order magnitude gravity anomalies extends in a northwest-southeast direction in the Hurgada – Shadwan – Ras Mohamed areas. This belt is

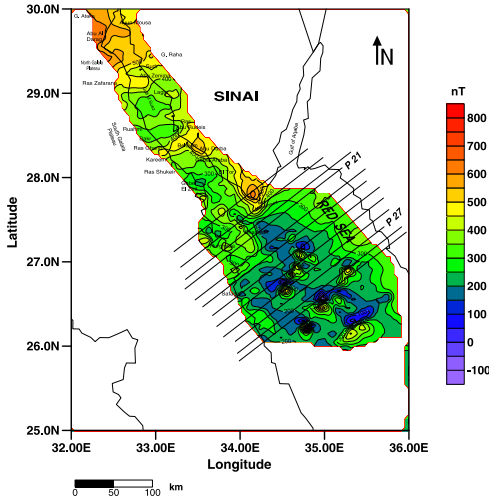


Fig. 6. RTP magnetic anomaly map of the Red Sea area. The profiles *P21–P27* represent the planes along the rift floor (contour interval 25 nT).

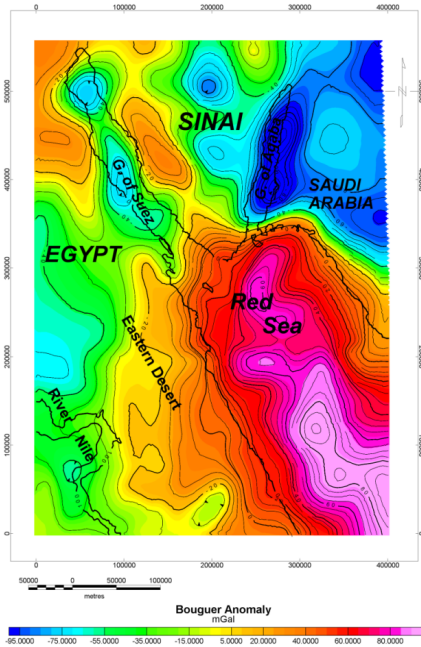


Fig. 7. The Bouguer anomaly map of the Red Sea area.

characterized by intensive gravity variations. It may be subdivided into the following three units:

1. Northern zone of the Gulf of Suez: This zone is characterised by first order gravity anomalies both in magnitude and size. The minimum value is about -50 mGal. It is bordered by a zone of intensive gravity variation within which the local gravity high of Ayun Musa gia is located.
2. Central zone of the Gulf of Suez: This zone is also associated with first order gravity low anomalies of about -80 mGal. It is distinctly bordered by the strips of intensive gravity variations of the meridian trend of Zafarana, Abu Rudeis-Belayim-Shukheir-Abun Zeneima areas. Within the axial part of the regional gravity low, local highs of the trend occurred at Ras Gharib, Kareem and Gharib north. These are associated with the Kareem-west Ruahmi low, which may form the Khashaba basin.
3. Southern zone of the Gulf of Suez: Gravity anomalies in this zone differ from those of the other zones of the gulf in being elongated in shape. They, like all others in the area between the Gulf of Suez and the Red Sea, follow the Clysmic trend.

The most dominant feature of the Bouguer map (Fig. 7) is a linear positive anomaly ($+80$ mGal) centered over the Red Sea, flanked by two small anomalies over the Arabian shield and over the Nubian shield). The total width of the anomalous zone is of an order of 300 km. It is obvious that, such a large-amplitude, long-wavelength anomalies cannot be produced solely by crustal inhomogeneities and a substantial contribution from subcrustal density variations (asthenosphere) should be expected.

4. Methods

4.1. Wave number filtering technique

Wavelength filtering was applied to the gravity and magnetic data for the purpose of detailed qualitative interpretation. This was done using the FFT

approach (*Degro, 1986*). In this study, we applied the 2D filtering to the RTP aeromagnetic maps, and Bouguer map to the lineation caused by structural faulting or dislocations in the basement rocks at different depths. The effective cut off wavelengths have been selected such that the depths of the mass centers of the causative bodies are in accordance with the results of 3D gravity and magnetic modeling.

The high-pass magnetic filtered map of the Southern Sinai area with effective wavelength at a depth of 3.0 km (Fig. 8) elucidates high frequency and short wavelength which are inferred as residual components located in the eastern and southeastern part of the studied area. The map contains a large numbers of smaller anomalies resulted from the filtering process. However, the main trends of the faults in the original magnetic map (trends of faults in the original magnetic map is NE–SW and NW–SE) are still present map and this indicates that the prominent fault trends extended in the subsurface up to shallow depths.

From a detailed analysis of low-magnetic filtered map with cut off at a depth of a approximately 3.0 km (Fig. 9) is clear that the prominent NE–SW and NW–SE anomalies trends still persist which reflects the deep extent of the subsurface structures causing these faults anomalies. However, some smooth regional anomalies that appear not to be related to a subsurface structure are most probably a result of regional variation in the magnetization or magnetic susceptibility of the rocks at the high depth.

Note the general shape of the existing subsurface structures in the area, until they reach a depth at which the full distortion and disappearance of the subsurface structures occur. We find that this takes place at depth of 11 km in high-pass filtered map (Fig. 10), and at depth of 25 km in low-pass magnetic filtered map (Fig. 11). This indicates that these anomalies are probably related to regional deep seated structures (deeper crust extending from approximately 11 km to a relative depth of 25 km).

The high-magnetic filtered map, of the Red Sea area, with cut-off at a depth of 30.0 km (Fig. 12), clearly shows two main types of northwest-trending magnetic anomalies within the offshore northern Red Sea. There is a group of linear, parallel-to-coastline magnetic anomalies, of reversed polarity and of very high frequency and strong amplitude (500–700 nT), which are discontinuous in nature and very similar to those anomalies associated with the axial trough of the central and northern Red Sea. At an

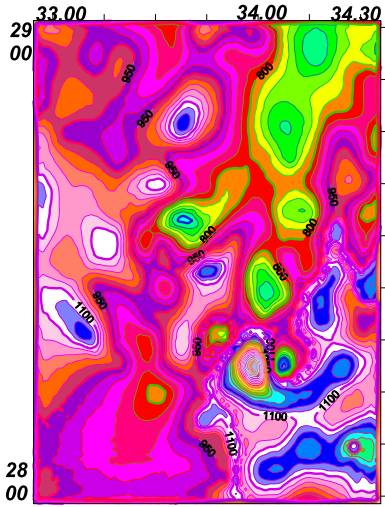


Fig. 8. High-pass magnetic filtered map of the Southern Sinai area with an effective cut-off wavelength of 3.0 km.

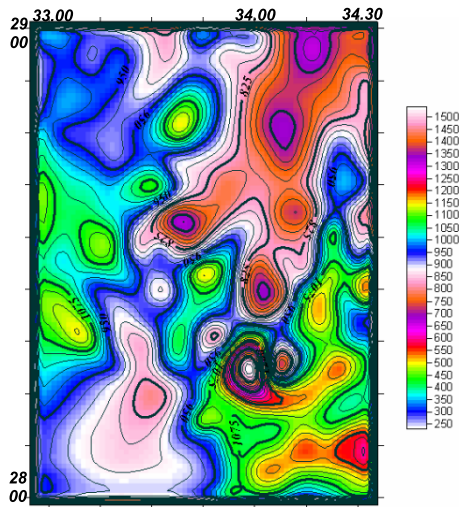


Fig. 9. Low-pass magnetic filtered map of the Southern Sinai area with an effective cut-off wavelength of 3.0 km.

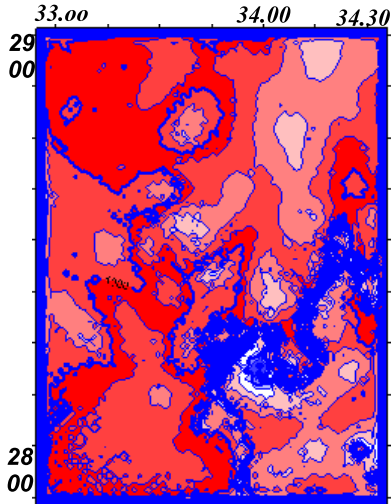


Fig. 10. High-pass magnetic filtered map of the Southern Sinai area with an effective cut-off wavelength of 11.0 km.

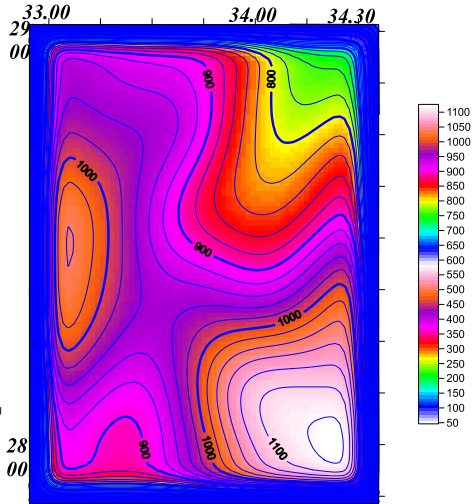


Fig. 11. Low-pass magnetic filtered map of the Southern Sinai area with an effective cut-off wavelength of 25.0 km.

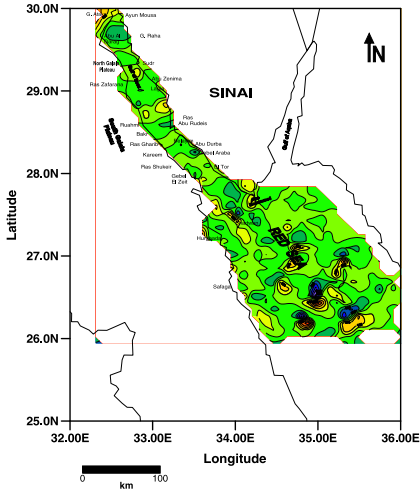


Fig. 12. High-pass magnetic filtered map of the Red Sea area with an effective cut-off wavelength of 30.0 km.

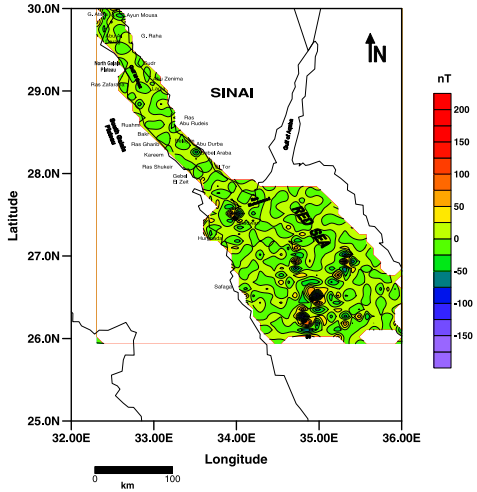


Fig. 13. High-pass magnetic filtered map of the Red Sea area with an effective cut-off wavelength of 12.8 km.

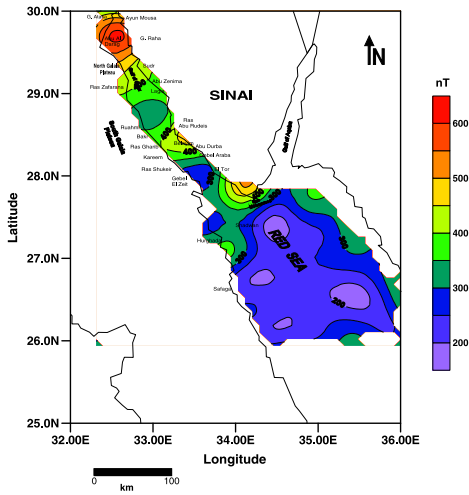


Fig. 14. Low-pass magnetic filtered map of the Red Sea area with an effective cut-off wavelength of 30.0 km.

effective cut-off wavelength of 12.8 km (Fig. 13), the high pass magnetic filtered map clearly shows two main types of northwest-trending magnetic anomalies within the offshore northern Red Sea. There is a group of linear parallel to coastline magnetic anomalies, of reversed polarity and of very high frequency and strong amplitude, which are discontinuous in nature and very similar to those anomalies associated with the axial trough of the central and northern Red Sea. The local anomaly structures are absent at this shallow depth, where no magnetic structure can be recognized.

From the analysis of low-pass magnetic filtered map of the Red Sea area shown in Fig. 14, with an effective cut-off wavelength at depth of 30.0 km, we find out that the magnetic field increases in the northeastern direction and with a maximum value at Abu Al Darag area with the prominent trends in NW–SE. The prominent structure trends in the original RTP magnetic map (Fig. 6), starting from the Ayun Musa and even El-Tor is still found in the low magnetic filtered map (Fig. 14) which reflects the tectonic nature of the faults and subsurface structures which extend from shallow depths and even greater depths.

We note also that the local structures in the southern zone starting from the Island of Shedwan and even latitude 26.00, clearly shown in RTP magnetic map (Fig. 6), are found to have disappear from the magnetic filtered map while regional structures for the same zone are still found. Interpretation can be given, however, in terms of residual local structures extending to a shallow depth while stretching regional structures to great depth and having a strong tectonic effect.

The low-pass gravity filtered map of the Red Sea area shown in Fig. 15 is a case with an effective cut-off wavelength with a depth of origin of 30 km. The main feature of this map is the NNW–SSE trend, where the gravity anomalies increase towards the Red Sea axial rift (eastern side). In the Red Sea area the anomaly values increase from -30 mGal (below the Red Sea mountains) to -5 mGal at the Red Sea coast. The elliptical negative anomaly below the Sinai region with a E–W trend indicates clearly the increase of the crustal thickness below the Sinai region. On the other hand, in the Red Sea axial depression the maximum value is $+60$ mGal due to a decrease in crustal thickness beneath the Red Sea. The high pass gravity filtered map with a depth of 30 km (Fig. 16), is very similar to the unfiltered Bouguer map, as shown in Fig. 7; additionally some isolated negative

anomalies can be seen along the Red Sea coast having a NW–SE trend and values of more than -10 mGal.

At a cut-off wavelength of 12.8 km (Fig. 17), the major regional trends become less clearly defined as they are now superimposed on each other. Small anomalies become clearly defined and nearly all the anomalies of the Bouguer map are represented. The high pass gravity filtered map (Fig. 18) shows that the local anomaly structures are absent at this shallow depth, where there is no local structure to be recognized.

The results of the filtering operations along the Red Sea area show that the regional gravity trend of the two main positive and negative anomalies persists between the cut-off wavelengths of 30.0 km and 12.80 km indicating that these anomalies are probably related to regional deep-seated structures (upper mantle and or deeper crust) extending from approximately 12.8 km to a relative depth of 30.0 km. This trend agrees well with the geological data interpretation and the seismic refraction data (*Said, 1962; Bayoumi, 1983; and Makris and Ginzburg, 1987*). These results are consisted with the results for the Moho depth map (Fig. 19) as obtained from the 3D modeling. The type of crust changes gradually from continental to oceanic, from north to south. The zone of crustal thinning coincides mostly with zones of low-density heated anomalous upper mantle beneath the rift floor (7 km). The eastern plateaus (the Red Sea hills) show by far the largest crustal thickness in the region (32 km). Also the analysis of map shows a relatively shallow depth of 18 km beneath the Gulf of Suez, and lies at a constant depth of 11–13 km at the northern Red Sea axial rift, indicating thinning of the Earth's crust in the northern Red Sea. The model also reveals a maximum Moho depth of about 37 and 35 km beneath both the Red Sea Hills and Sinai Mountains, respectively.

4.2. 3D gravity and magnetic modeling

4.2.1. 3D gravity modeling

The 3D forward gravity modeling package IGMAS (Interactive Gravity Analyzing System), developed by *Schmidt and Götze (1998)* was used to establish the geometry and density distributions of the rift. The method is based mainly on transforming the volume integrals involved in the verti-

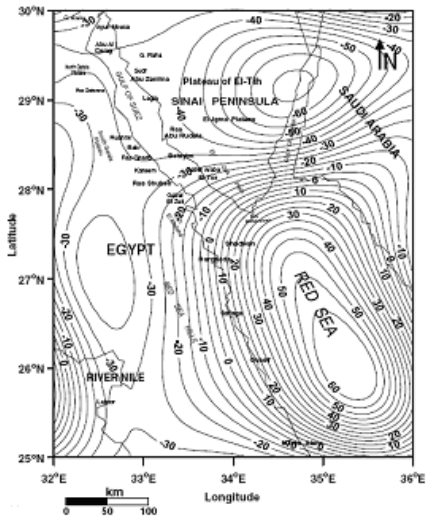


Fig. 15. Low-pass gravity filtered map of the Red Sea area with an effective cut-off wavelength at depth of 30.0 km.

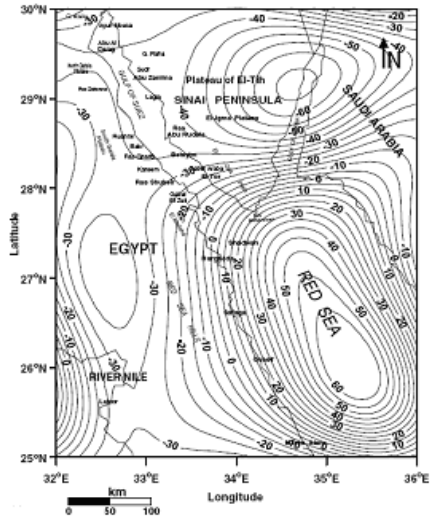


Fig. 16. High-pass gravity filtered map of the Red Sea area with an effective cut-off wavelength at depth of 30.0 km.

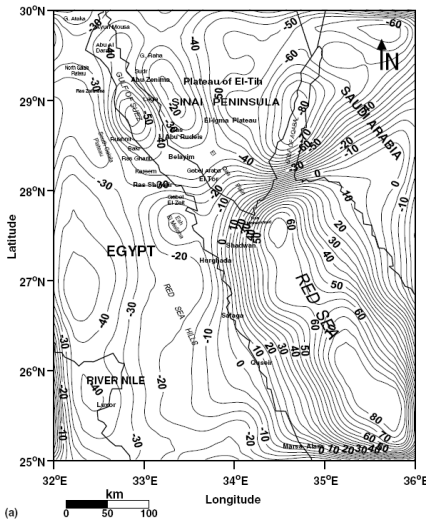


Fig. 17. Low-pass gravity filtered map of the Red Sea area with an effective cut-off wavelength at depth of 12.8 km.

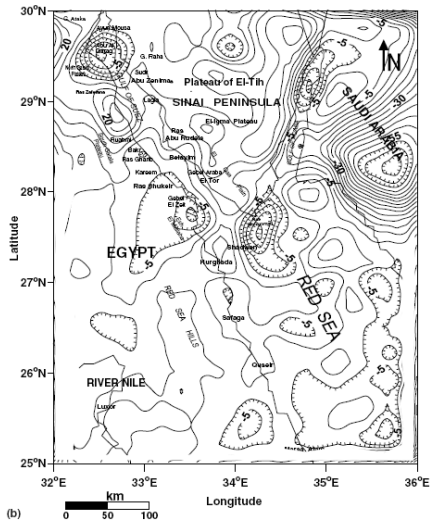


Fig. 18. High-pass gravity filtered map of the Red Sea area with an effective cut-off wavelength at depth of 12.8 km.

cal attraction of a homogeneous polyhedron into a sum of line integrals suitable for computer programming. The program requires an input data structure along a definite number of vertical modeling planes perpendicular to the general geological strike, with the vertices of the assumed subsurface structures interconnected to form a line separating two media with different densities. The model also gives a more realistic approximation of the geological structures (*Götze, 1976, 1984; Götze and Lahmeyer, 1988*). Since the general geological strike along the rift floor is variable, the 3D modeling was applied along the Red sea area. The location and orientation of the vertical modeling planes are shown in Fig. 20. The vertical planes are parallel to each other, and the distances between the planes are variable along the rift floor depending on the location of the anomalies, on the Bouguer map, and their corresponding causative bodies, and on the geological map.

4.2.2. 3D magnetic modeling

The density values were constrained as before by compressional velocities using the Nafe and Drake empirical function for the sediments (*Nafe and Drake, 1957*) and the Birch relationship (*Birch, 1961*) for the igneous crust; magnetic susceptibilities were constrained by densities (*Schön, 1983*). The region for which the 3D magnetic modeling was applied is shown in Fig. 20. The magnetic profiles were selected along the same profiles as in the gravity model for the northern Red Sea. The magnetic data will only reveal information on the part of the crust for depths with temperatures above the Curie isotherm. The dominant magnetic mineral in the crust is regarded to be magnetite, which has a Curie temperature of up to 578 °C (*Merrill and McElhinny, 1983*). Thermal gradients of 46 °C/km and 76 °C/km are typical for continental and oceanic crusts, respectively. These gradients place the Curie isotherms at depths of around 12 km and 8 km (*Morgan et al., 1985; Schutz, 1994*). As the cause for the high frequency magnetic anomaly is shallow in origin, most of the geometrical modifications done to the model were on the igneous crust and partly on the upper crust-sedimentary interface.

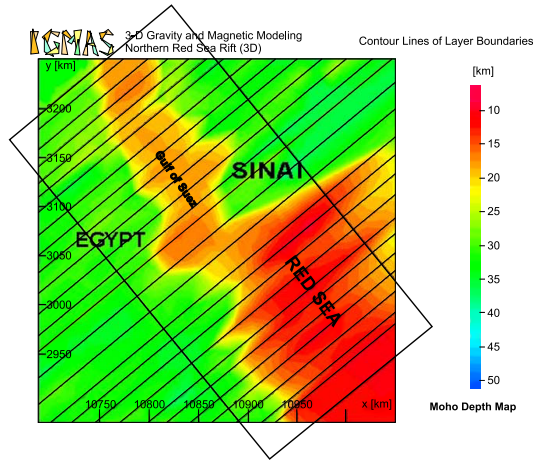


Fig. 19. Moho depth map for the studied areas.

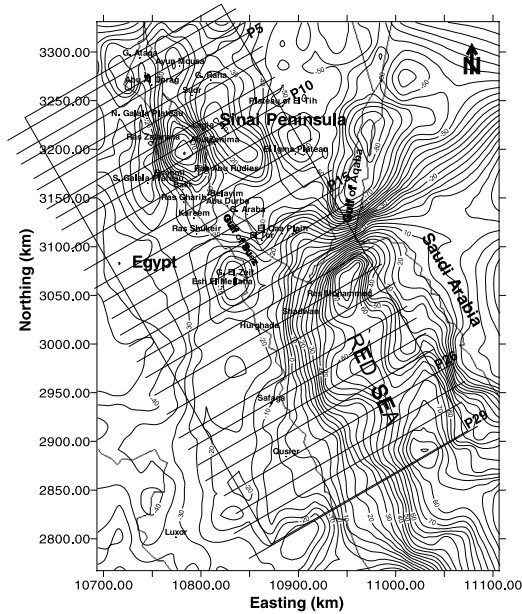
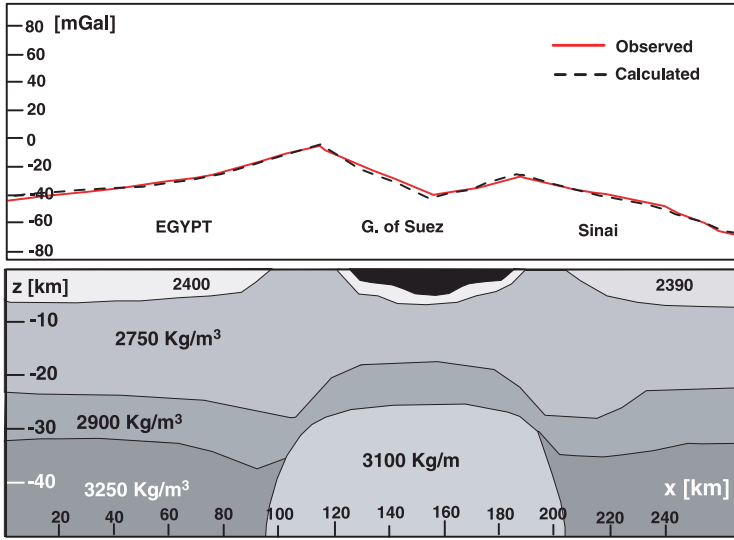
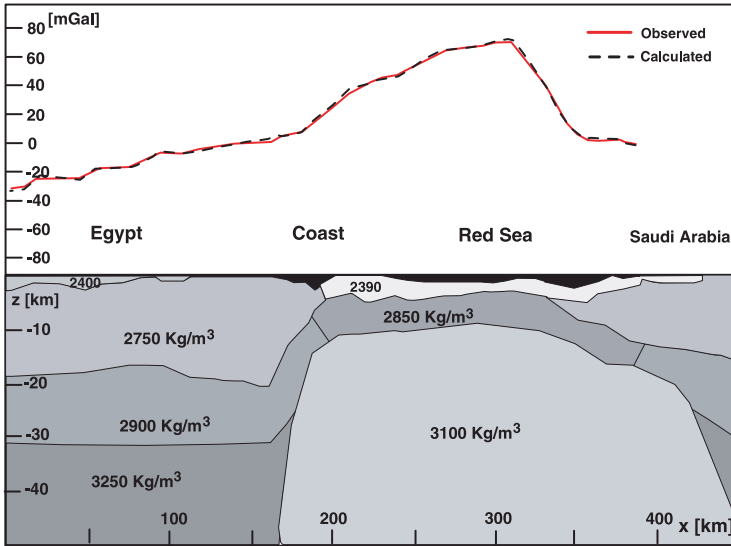


Fig 20. Location map of gravity and magnetic modeling. The magnetic profiles were selected along the same profiles as in the gravity model. The profiles *P10*, *P15* and *P26* (bold) are illustrated at places at which the phenomenon of the poleward younging of continuous and discontinuous spreading ridges was recorded from the northern part of the Red Sea.



(a)



(b)

Fig. 21. (a) The vertical cross-section of the 3D gravity model from the central sector of the Red Sea region, along plane 15 and (b) the vertical cross section of the 3D gravity model from the Southern sector of the Red Sea region, along plane 26.

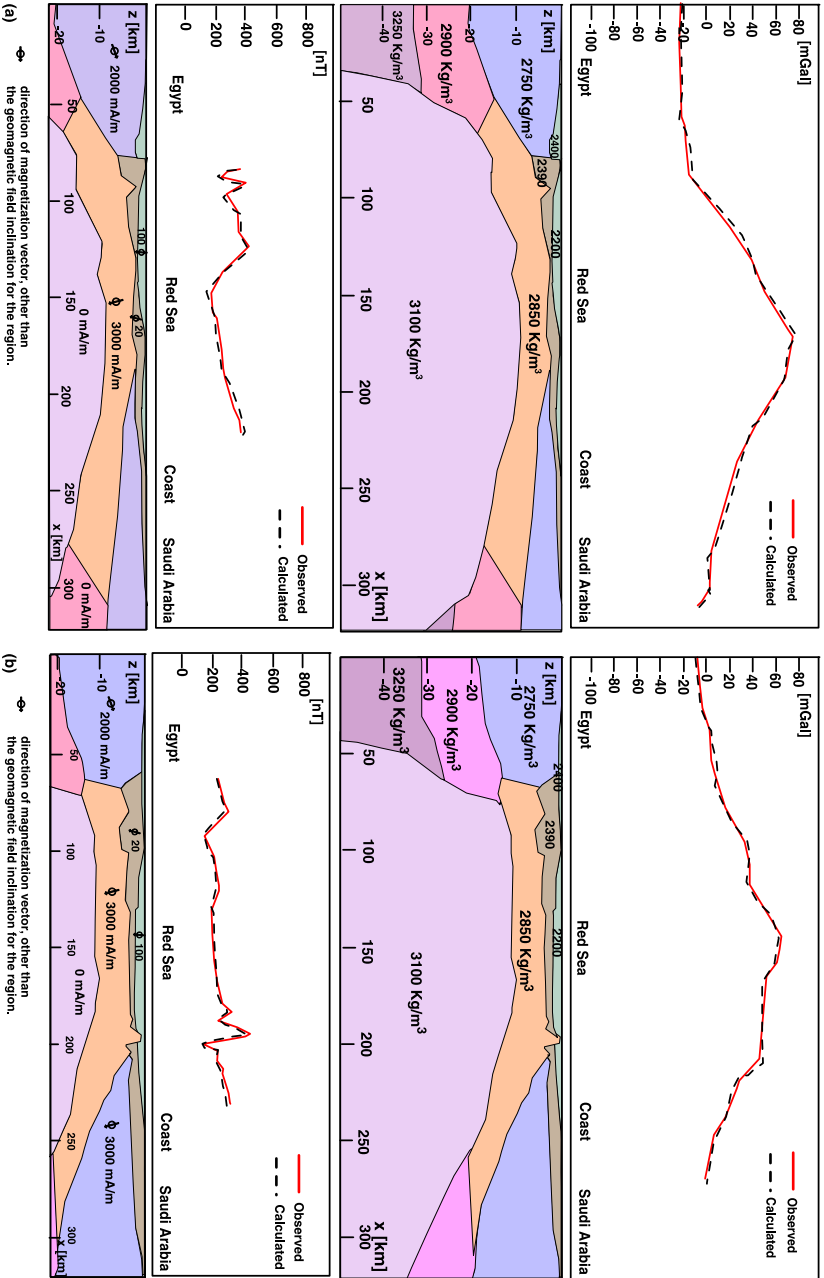


Fig. 22. (a) The vertical cross-section of the 3D gravity and magnetic model from the northern part of the main rift (plane 21) and (b) the vertical cross-section of the 3D gravity and magnetic model from the northern part of the main rift (plane 27).

5. Results

5.1. Analyzing the results of 3D magnetic and gravity models, and clarifying their structural indication

The initial model for the gross crustal structure of the Red Sea and Suez rift consists of eight bodies representing different lithological and tectonic units. A section from the central sector of the Red Sea is shown in Fig. 21 (for the locations of the modeling planes refer to Fig. 20). The long-wavelength gravity anomalies along the axial portion of the northern Red Sea rift floor is best explained in terms of a relatively low density upper mantle ($\rho = 3100 \text{ kg/m}^3$). Its comparable seismic velocity equals to 7.5 km/s which was investigated along the axial Red Sea and Suez rifts (*Gaulier et al., 1988*). This anomalous layer seems to cover large parts of the main Red Sea axial rift. This low velocity anomalous upper mantle could reflect a change in the P-T conditions (pressure release and convection heat) of the Moho and the decrease of VP could be estimated to be 0.1 km/s (*Anderson et al., 1968*). The results, from magnetic and gravity models (Figs. 21 and 22) demonstrates that the P-T parameters cannot explain the low mantle velocity of 7.5 km/s (*Gaulier et al., 1988*) measured beneath the Gulf of Suez. Attenuation of seismic waves with distance increases sharply from the coast to the axial area. This attenuation may be related to active fracturing and/or to higher temperatures which may indicate the presence of partial melting at depth. Hence, the previous mechanisms, related to active fracturing and/or to higher temperatures, may indicate the presence of partial melting at great depths. The lateral density variations in the upper mantle seem to be extremely intense in the coastal zone of the Red Sea, the low-density material is confined exclusively to the rifted area. This result is very similar to the findings of *Makris and Ginzburg (1987)* for the southern Red Sea. It should be noted that the aerial extent and degree of doming of basement crystal rocks (upper igneous crust) are far greater on both sides of the Red Sea rift than that of those bounding the Suez rift; furthermore the distribution of outcropping basement rocks is limited only to the southern half of the Gulf of Suez. This suggests that the rate of rifting in the Red Sea is greater than that in the southern half of the Gulf of Suez, which in turn suffered more rifting than in the northern half of the Gulf. On the other hand, as mentioned before, the negative residual anomaly is attributed to

the sediments of the Suez rift. This negative residual anomaly is well explained with a density value of 2220 kg/m^3 , 2390 kg/m^3 and 2400 kg/m^3 attached to the recent, evaporitic series and anhydrite rocks, respectively. The total thickness of the sediments in the Suez rift, as obtained from the gravity modeling, is over 7 km (Fig. 21). The thickness of the sediment, though sparsely deposited, increases towards the central part of the Red Sea and Suez rifts. The upper continental crust (crystalline basement), which is considered here at the bottom of the sedimentary layer, was modeled with a mean density value of 2750 kg/m^3 . Beneath the Gulf of Suez, the top interface of the crystalline basement (upper crust) is generally marked by the maximum thickness of the sedimentary layer (over 7 km, compare Fig. 21a and 21b). The thickness of the upper crust is about 2 km under the central sector of the Suez rift. This generally thickens towards the adjoining plateaus (eastwards to Red Sea Hills and westwards to the Sinai Mountains). The maximum thickness of the upper crust was found beneath both Sinai Mountains and Red Sea Hills, where the basement rocks crop out, and have a thickness of 23 km (Figs. 21b and 22a). The lower continental crust has been modeled with a density value of 2900 kg/m^3 . Because of the asthenospheric uplift beneath the Gulf of Suez and rifting taking place, the bottom interface of this layer with the upper mantle has a minimum depth of about 18 km. As a result of pressure release and convection heat, indicating a more advanced stage of rifting taking place in the northern part of Red Sea rift, the uplift and rifting are interpreted as an evidence for updoming due to the sea floor spreading in the central Red Sea (*Bosworth and Strecker, 1997*). The crustal rocks become chiefly oceanic and consist of basalts. The model shows that the top of this oceanic crust in the axial area of the Red Sea is relatively flat at a mean depth of 7–8 km. The minimum thickness of oceanic crust has been observed, due to the more advanced stage of rifting, to be 5 km (Fig. 21b). The model shows also the presence of a steep increase in crustal thickness towards the continent below the coastal plain.

Magnetic modeling (Figs. 22a and 22b) shows a poor flattening, especially in the eastern region. This is contrary to what is given by other authors (e.g., *Gaulier et al., 1988*). However, the present results are in good agreement with the geothermal gradient values in the Red Sea (*Cochran et al., 1986*). Parameters are reasonable (Fig. 22a and 22b). The phenomenon of the poleward younging of continuous and discontinuous spreading ridges

was recorded from the northern part of the Red Sea as shown in Fig. 20 which illustrates the positions where this phenomenon was recorded in the Northern Red Sea. *Courtillot et al. (1979)* explained the phenomenon as the manifestation of a poleward axial propagation of a lithospheric crack. *Bonatti (1985)*, described the phenomenon as punctiform initiation of seafloor spreading over hot areas which are related to mantle thermal waves and whose activation shows a poleward time progression. Bonatti model suggests that the recent spreading has been about 0.5 cm/yr.

5.2. Seismicity of Southern Sinai and Red Sea areas

Recently, great efforts have been taken to explore the Southern Sinai and the Red Sea area, especially Hurgada, Ras Alem, Sharm El-Shikh town for touristic activity, also the historical places in Moses Mountain and Sant Catrin. Therefore, due to the importance of this area, some light should be thrown on the seismicity and its relationship to local tectonics. The seismicity map of the area was constructed for the time period 1906–2003 covering values ≥ 3.4 (Fig. 23). The map showed that the energy release along the Red Sea appeared to be connected with those in the Southern Sinai, suggesting a tectonic connection between these regions and the Red Sea. To understand this pattern of seismicity (Fig. 23) and the interconnection of different tectonic areas, the whole area can be divided according to the seismic activity into three main zones. These include the Northern Red sea with the Gulf of Suez, the Central Red Sea and the Southern Red Sea. We will explain the tectonic activity in each zone and its relationship to the general tectonic in the region.

The Northern Red Sea and Gulf of Suez zone were studied in the papers *Cochran (1983)*, *Daggett et al. (1986)* and *Girdier and Southern (1987)*. Some of these studies showed that the northern Red Sea has been affected by the mid axial rift which has been shifted toward the Gulf of Suez. The distributions of the earthquake epicentres show high activity at the entrance of the Gulf of Suez. This activity has been attributed to relative motion between Sinai Arabian and African plates. Some geologic tectonic and focal mechanism studies suggest the dominance of the northern part of the Gulf of Suez by right lateral shearing stresses (*Korrat et al., 1990*). Tectonically the northern Red Sea is still dominated by extensional stresses in a nearly

NNE–SSW direction (*Hempton, 1987*).

The central Red Sea appears to be seismically quiet, representing a balanced zone between the active southern and northern Red Sea zones (*Martinez and Cochran, 1988*). Only four events with magnitudes < 4.0 were recorded (*Daggett et al., 1986*) within the considered period (1906–1989). Many authors (*Backer and Schoell, 1972; Girdler, 1985*) studied this part using different geophysical tools, revealing that the Mid axial rift is discontinuous in the central Red Sea. Geological studies showed that the central Red Sea is bounded by two major fault systems. These two fault systems probably isolate the central part of the Red Sea releasing energy outside and leaving it in an equilibrium state. As a result, the central Red Sea appeared as a quiet zone.

The spatial distribution of recent activity in the southern Red Sea showed that the activity is concentrated along the rift valley. Two cluster points appear in this zone near latitude 17° and 20°N where activity is higher than in the surrounding area. Between these two points, active sea floor spreading has directions of motions along the Afro-Arabian rift which is active nowadays with maximum activity at the intersection of two or more structural elements. *Kebede and Kulhánek (1991)* established a tentative model (Fig. 24) for the major tectonic elements affecting the Red Sea and Southern Sinai areas based on the results of epicentral distribution focal mechanism solution, and seismic energy release studies. In general recent seismicity takes the trends of major tectonic and structural elements.

El-Sayed et al. (2001) created a map showing the seismic hazard zones and earthquakes in Egypt using the spatial distribution of recorded earthquakes (Fig. 25) to identify the major seismic zones and seismic zones with common focal mechanisms. Lines denote the major tectonic elements and seismic zones with focal mechanisms in Egypt and its vicinity: 1. Gulf of Aqaba–Levant; 2. Northern Red Sea–Gulf of Suez; 3. Suez – Cairo – Alexandria; 4. Eastern Mediterranean – Cairo – Fayoum; 5. Mediterranean costal; 6. Aswan and Quena zone.

Several large recent and historical earthquakes occurred along these zones. The largest magnitude event of 7.3 took place in the Gulf of Aqaba on November 22, 1995. *Abdel Rahman (2009)*, *Fergani et al. (2007)*, *Korrat et al. (2006)*, *El-Hefnawy et al. (2006)* have made serious attempts to explore and follow seismic belts in Egypt. The results obtained were close to the

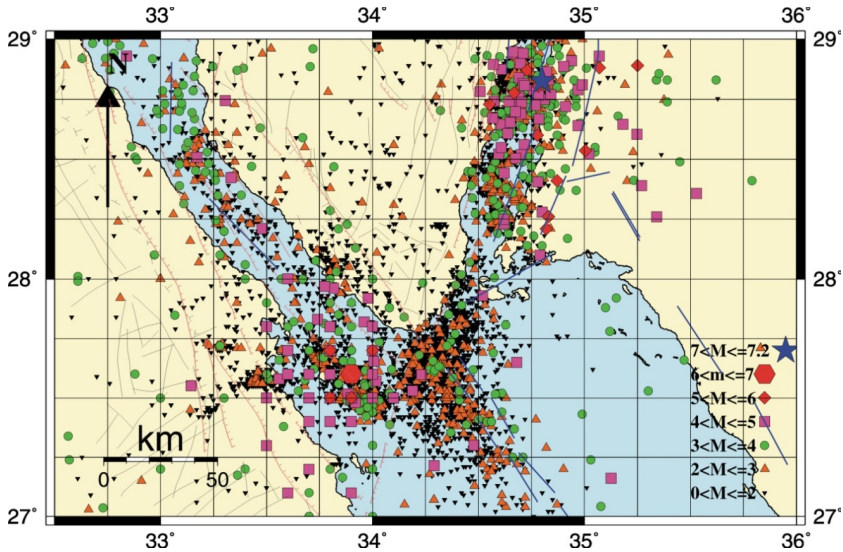


Fig. 23. Seismicity of the Southern Sinai and Red Sea areas.

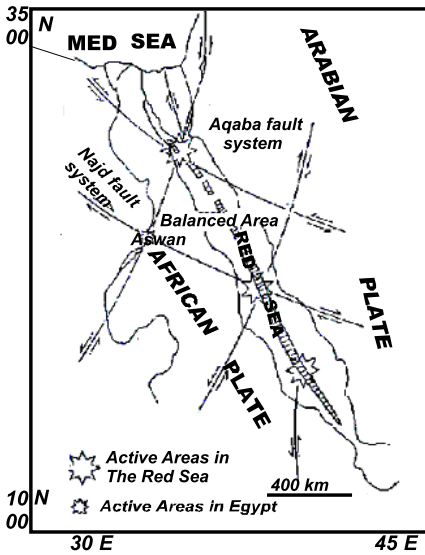


Fig. 24. A tentative model for the major tectonic elements effecting the Red Sea and Southern Sinai areas (modified after Kebede and Kulhánek, 1991).

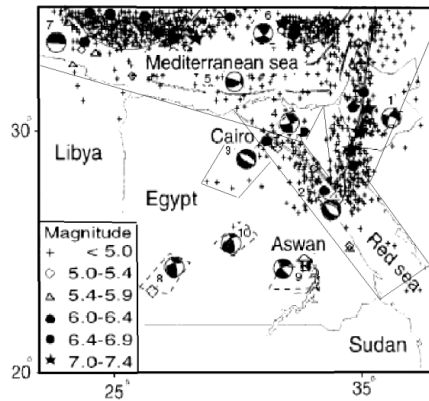


Fig. 25. Location map of earthquakes and seismogenic zones in Egypt (El-Sayed et al., 2001).

results inferred by *El-Sayed et al. (2001)*. The Gulf of Suez is characterized by a moderated earthquake activity. The March 1969 earthquake was the strongest recent earthquake ($M = 6.6$) and its hypocenter was located at Shadawn Island in the southern entrance of the Suez Gulf (*Maamoun et al., 1984*). Intermediated magnitude seismicity occurs in the northern Red Sea. *El-Isa and Al Shanti (1989)* reported that in the period 1913–1986 about 135 events ($3 \leq M \leq 6.9$) occurred in the Red Sea and western Arabia peninsula between latitudes 14° and 27.2°N .

The Red Sea rift trends NNW–SSE and extends south of Sinai Peninsula between north Africa and Arabian Peninsula. It has been formed by the separation of the Arabian plate from African continent (*McKenzie et al., 1970*). Bathymetry and gravity data demonstrate that the Aqaba shear fault extends southwards to the southern extremity of the Sinai Peninsula. *Makris and Rihm (1991)* proposed a pull-apart model for explaining the seismotectonic activity of the Red Sea and some parts of Gulf of Aqaba. This model includes also gradual thinning of the continental crust, heat flow, uplift of the near slope parts and increasing subsidence of the graben floor during the process of rifting observations.

The crustal structure of the Red Sea area has been extensively studied by many researchers, in an attempt to explore the subsurface structure of the area as well as the relationship between tectonic activity and compositional form. *Avedik et al. (1988)* and *Gaulier et al. (1988)* estimated the Moho depth to be between 11.5 and 18 km based on refraction studies. On the other hand, other geophysical results indicate that, it is around 20 km near the shore line and ranges from 35 to 40 km in the land area (*Tramontini and Davies, 1969; Makris et al., 1983*). This inference is consistent with the results of *Prodehl et al. (1997)*.

6. Conclusions

The purpose of our study has been the transformation and interpretation of the RTP aeromagnetic data, gravity data and seismic data of the southern Sinai and Red Sea areas to evaluate the subsurface active structures affecting both the sedimentary section and the underlying basement complex. Based on the the results we have obtained, we can make the following conclusions:

1. A detailed analysis of the RTP aeromagnetic anomaly maps of the Southern Sinai and the Red Sea areas (Figs. 5 and 6) clearly shows that the major structural trends in each of the two areas are NW–SE and NE–SW. The map (Fig. 5) shows a strong positive anomalies concentrated in three key areas that are located in the western, central and southeastern parts of the Southern Sinai. The strong magnetic anomalies in these parts may be attributed to the occurrence of subsurface basic intrusions of high magnetic content. The RTP aeromagnetic anomaly map of the Red Sea area (Fig. 6) reveals that the part is located in the far northwestern of the Red Sea coast characterized by the elongated anomaly zones with steep gradient and closures and indicates considerable subsurface faulting with NW–SE trending. These anomalies are most probably related to basement faulting structure. The most dominant feature of the Bouguer anomaly map of the Red Sea area (Fig. 7) is a linear positive anomaly centered over the Red Sea flanked by two small anomalies over the Arabian shield and over the Nubian shield. The total width of the anomalous zone is about 300 km. It is obvious that such a large-amplitude, long-wavelength anomalies cannot be produced solely by crustal inhomogeneities and a substantial contribution from subcrustal density variations (asthenosphere) should be expected.
2. The results of the filtering operations along the Red Sea area show that the regional trend of the two main positive and negative anomalies persists at a depth of 30 km indicating that these anomalies are probably related to regional deep seated structures (upper mantle and/or deeper crust) extending from approximately 12.6 km to a depth of 30 km. The filtering operations have been applied to magnetic data of the Southern Sinai trying to isolate superimposed effects especially in the Gulf of Suez area. It was possible to eliminate short wavelength anomalies, which are probably related to sedimentary layers at the depths lower than 7 km. The results indicate that the regional deep seated structures (deeper crust) extend from approximately 11 km to a depth of 25 km. These results agree well with the geological data interpretation and the seismic refraction data (*Said, 1962; Bayoumi, 1983 and Makris and Ginzburg, 1987*).

3. Combined 3D gravity and magnetic models are presented in this study. The studied models reveal the existence of hot upper mantle material beneath the Red Sea rift floor. The 3D gravity model evaluates the density distributions of the deep lithospheric structures of the Red Sea rift. The magnetic data analysis reveals the topography of the oceanic crust and intra-crustal inhomogeneities within it. Moreover, the magnetic anomalies reflect the sea floor spreading rate. The combination of gravity and magnetic data analyses has improved the geometry and the density distribution in the 3D calculated profiles. Our results provide an important contribution towards the inferred nature and state of the crustal structure of the rift. On the Red Sea coast the changes in the crust, sediment cover and upper mantle are very intense as obtained from the 3D gravity modeling. On the Red Sea coast the crust is still continental only 21 km thick and, at least in some areas covered by thick sediments.

The relatively low density of the anomalous upper mantle (3100 kg/m^3) of the Red Sea rift as deduced from the gravity modeling indicates the possible presence of partial melting in the upper mantle. The size of the area of anomalous upper mantle suggests that a large scale asthenospheric upwelling might be responsible for the subsequent rifting of the Red Sea. These results are in agreement with Cochran's concept of the northern part of the Red Sea (*Cochran and Martinez, 1988*). The lateral density variations in the upper mantle seem to be extremely intense in the coastal zone of the Red Sea, with low density material being confined exclusively to the rifted area. This result is based on *Makris et al. (1988)* and is very similar to the finding of *Makris and Ginzburg (1987)*, *Cochran and Martinez (1988)* and *Martinez and Cochran (1988)* for the northern Red Sea. The interpretation of magnetic data of the Red Sea rift shows that the spreading rate of the part south of latitude 26.5°N agrees well with the theoretical model in the order of 0.7 cm/yr .

4. Analysis of the the seismicity map of the studied areas, which was performed for the time period 1906–2003 covering values > 3.4 , leads to a conclusion that the southern Red Sea and the northern Red Sea including Shadwan area (Fig. 23) showing high values of energy release. The northern Red Sea has been affected by the mid axial rift which

has been shifted toward the Gulf of Suez. The Red Sea rift trends NNW–SSE and extends South of Sinai Peninsula between north Africa and Arabian Peninsula. It has been formed by the separation of the Arabian plate from African Continent (*McKenzie et al., 1970*).

The present seismic activity is mainly concentrated along the three main fault systems reaching a maximum in the Aqaba-Levant area (Fig. 24). The Red Sea – Gulf of Suez zone gives dominantly normal faulting mechanism except the northern half of the Gulf of Suez which is probably dominated by a strike slip mechanism. The trend displayed by the Sinai sites being rather uniform and different from those located on the west shore of the Gulf of Suez gives geodetic evidence of the sub-plate behavior of the Sinai peninsula with respect to African plate. The earthquake distribution pattern in Fig. 23 shows high activity at the entrance of the Gulf of Suez. This activity is attributed either to the intersection of the mid-axial rift with the boundaries of Sinai Subplate or to interactions due to relative motion between Sinai Arabian and African plates.

Acknowledgments. Dr. L. Brimich is grateful to the Slovak Grant Agency VEGA (grant No. 2/0067/12 for partial support of the work.

References

- Abdallah A. M., Abu Khadra A. M., 1976: Remark on the geomorphology of the Sinai Peninsula and its associated rock, Egypt. Geol. Surv., Egypt.
- Abdel-Rahman K., Al-Amri A., Abdel-Mneim E., 2009: Seismicity of Sinai Peninsula, Egypt. Arab. J. Geoscience, **2**, 103–118.
- Anderson O. L., Schreiber E., Lieberman R. C., Soga N., 1968: Some elastic constant data on minerals relevant to geophysics. Rev. Geophys., **6**, 4, 491–524.
- Avedik F., Geli L., Gauller J. M., Le-Formal J. P., 1988: Results from three refraction profiles in the northern Red Sea recorded with Oceanic bottom vertical seismic Array. Tectonophysics, **153**, 89–101.
- Backer H., Schoell M., 1972: New deeps with brines and metalliferous sediments in the Red Sea Nature (London). Phys. Sci., **240**, 153–158.
- Bayoumi A. J., 1983: Tectonic origin of the Gulf of Suez, Egypt, as deduced from gravity data. In: Geyer R. A., Moore J. R. (Eds.), Handbook of Geophysical Exploration at Sea. CRC, 417–432.

- Birch F., 1961: The velocity of compressional waves in rocks to 10 kilobars. *J. Geophys. Res.*, **66**, 2199–2224.
- Bonatti E., 1985: Punctiform initiation of seafloor spreading in the Red Sea during transition from a continental to an oceanic rift. *Nature*, **316**, 33–37.
- Bosworth W., Strecker M., 1997: Stress field changes in the afro-arabian rift system during the Miocene to recent period. *Tectonophysics*, **278**, 47–62.
- Cochran J., 1983: A Model for Development of Red Sea. *Am. Assoc. Pet. Geol.*, **67**, 41–69.
- Cochran J. R., Martinez F., Steckler M. S., Hobart M. A., 1986: Conrad deep: a new northern Red Sea deep. Origin and implications of continental rifting. *Earth Planet Sci. Lett.*, **78**, 18–32.
- Cochran J. R., Martinez F., 1988: Evidence from the northern Red Sea on the transition from continental to oceanic rifting. *Tectonophysics*, **153**, 25–53.
- Courtillot V., Gadeano A., Le Mouel J. L., 1979: Propagation of an accreting plate boundary: a discussion of new aeromagnetic data in the Gulf of Tadjourah and southern Afar. *Earth Planet Sci. Lett.*, **47**, 144–160.
- Daggett P., Morgan P., Boulos F., Hennin S., El-Sherif A., El-Sayed A., Basta N., Melek Y., 1986: Seismicity and active tectonic of the Egyptian Red Sea margin and northern Red Sea. *Tectonophysics*, **125**, 313–324.
- Degro T., 1986: Zür Interpretation gravimetrischer und magnetischer Feldgrößen mit Hilfe von Übertragungsfunktionen. Dissertation, Institut für Geophysik der TU Clausthal, 139 p. (unpublished).
- Drake C. L., Girdler R. W., 1964: A geophysical study of the Red Sea. *Geophys. J. R. Astron. Soc.*, **8**, 473–495.
- Egyptian Geological Survey, 1994: Geological map of Sinai, Arab Republic of Egypt. Scale 1:250 000.
- El-Gezeery M. V., Marsouk I. M., 1974: Miocene rock stratigraphy of Egypt. *Egypt. J. Geol.*, **18**, 1–59.
- El-Hefnawy M., Deif A., El-Hemamy S., Gomaa N., 2006: Probabilistic assessment of earthquake hazard in Sinai in relation to the seismicity in the eastern Mediterranean region. *Bull. Eng. Geol. Env.*, **65**, 309–319.
- El-Isa Z., Al-Shanti A., 1989: Seismicity and tectonic of the Red Sea and western Arabia. *Geophysical Journal*, **97**, 449–457.
- El-Sayed A., Vaccari F., Panza G., 2001: Deterministic seismic hazard in Egypt. *Geophys. J. Int.*, **144**, 555–567.
- Fergany E., Oth A., Wenzel F., 2007: Synthetic of strong ground motion for $M = 7.2$ earthquake in the Gulf of Aqaba, Sinai-Egypt. *NRIAG J. of Geophysics*, **6**, 81–95.
- Gaulier J. M., Le Pichon X., Lyberis N., Avedik F., Geli L., Moretti, I., Deschamps A., Salah Hafez, 1988: Seismic study of the crust of the northern Red Sea and Gulf of Suez. *Tectonophysics*, **153**, 55–88.
- General Petroleum Corporation, A. S. R. T., 1980: Bouguer gravity map of Egypt. Scale 1:500 000.

- General Petroleum Corporation, A. S. R. T., 1990: Aeromagnetic map of Egypt. Scale 1:500 000.
- Geosoft program, 2008: Oasis Montage, software Package geosoft. Inc., U.S.A. Egyptian Geological Survey, 1994. Geological map of Sinai, Arab Republic of Egypt. Scale 1:250 000.
- Girdler R., 1985: Problems concerning the evolution of oceanic lithosphere in the northern Red Sea. *Tectonophysics*, **116**, 109–122.
- Girdler R., Southern T., 1987: Structure and evolution of the northern Red Sea. *Nature*, **330**, 716–721.
- Götze H. J., 1976: Ein numerisches Verfahren zur Berechnung der gravimetrischen und magnetischen Feldgrößen für 3D Moedellkörper. Dissertation, TU Clausthal (in German).
- Götze H. J., 1984: Über den Einsatz interaktiver Computergrafik in Rahmen 3D Interpretationstechniken in Gravimetrie und Magnetik. Habilitationsschrift, TU Clausthal, 236 p. (in German).
- Götze H. J., Lahmeyer B., 1988: Application of 3D interactive modeling in gravity and magnetics. *Geophysics*, **53**, 1096–1108.
- Hempton M., 1987: Constraints on Arabian plate motion and extensional history of the Red Sea. *Tectonics*, **6**, 687–705.
- Ismail A., Sultan A., Mohamady M., 2001: Bouguer and total magnetic intensity maps of Sinai Peninsula. Scale 1:500 000. Proceedings of the 2nd Int. symposium on Geophysics, Tanta, 111–117.
- Kebede F., Kulhánek O., 1991: Recent seismicity of the East African Rift system and its implications. *Physics of the Earth and Planetary Interiors*, **68**, 259–273.
- Korrat I., El-Gamili M., Albert R., Mousa H., 1990: Seismicity and its implication to the geologic setting of northern Egypt. 9th Symp. Quaternary and Development in Egypt. El-Mansoura (Abs.)
- Korrat I., Hussein H., Marzouk I., Ibrahim E., Abdel-Fattah A., Hurukawa N., 2006: Seismicity of the northernmost part of the Red Sea (1995–1999). *Acta Geophysica*, **54**, 1, 33–49.
- Mamoun M., Megahed A., Allam A., 1984: Seismicity of Egypt, HIAG, IV, 109–160.
- Makris J., Rihm R., 1991: Shear – controlled evolution of the Red Sea: pull-apart model. *Tectonophysics*, **198**, 441–466.
- Makris J., Allam A., Moktar T., Basahel A., Dehghani G. A., Bazari M., 1983: Crustal structure at the northwestern region of the Arabian shield and its transition to the Red Sea. *Bull. Fac. Earth Sci. K. Abdulaziz Univ.*, **6**, 435–447.
- Makris J., Ginzburg A., 1987: The afar depression: transition between continental rifting and sea-floor spreading. *Tectonophysics*, **141**, 199–214.
- Makris J., Rihm R., 1991: Shear-controlled evolution of the Red Sea: pull-apart model. *Tectonophysics*, **198**, 441–466.
- Makris J., Rihm R., Allam A., 1988: Some Geophysical aspects of the evolution and structure of the crust in Egypt. In: Greiling R. O., El-Gaby S. (Eds.) *The Pan-African Belt of Northeast Africa and Adjacent Areas, Tectonic Evolution and Economic*

- Aspects of a Late Proterozoic Orogen: Braunschweig, Friedr. Vieweg & Sohn, 345–369.
- Martinez F., Cochran J. R., 1988: Structure and tectonics of the northern Red Sea: catching a continental margin between rifting and drifting. *Tectonophysics*, **150**, 1–32.
- Mcknezie D., Davies D., Molnar P., 1970: Plate tectonic of the Red Sea and East Africa. *Nature*, **226**, 243–248.
- Merrill R. T., McElhinny M. W., 1983: *The Earth's Magnetic Field*. Academic Press, London, 401 p.
- Morgan P., Boulos F. K., Hennin S. F., El-Sherif A. A., El Sayed A. A., Basta N. Z., Melek Y. S., 1985: Heat flow in Eastern Egypt: the thermal signature of continental breakup. *J. Geodyn.*, **4**, 107–131.
- Nafe J. E., Drake C. L., 1957: Variations with depth in shallow and deep water marine sediments of porosity, density and the velocities of compression and shear waves. *Geophysics*, **22**, 523–552.
- Prodehl C., Fuchs K., Mechie J., 1997: Seismic refraction studies of the Afro-Arabian Rift system abrief review. *Tectonophysics*, **278**, 1–13.
- Rosser H. A., 1975: A detailed magnetic survey of the southern Red Sea. *J. Biochem.*, **13**, 131–153.
- Said R., 1962: *The Geology of Egypt*. Elsevier Publ. Co., Amsterdam and New York.
- Said R., 1990: *The Geology of Egypt*, 2nd edition Balkema, Rotterdam, 439–449.
- Schmidt S., Götze H. J., 1998: Program Documentation IGMAS. Institut für Geologie, Geophysik und Geoinformatik der FU Berlin, unveröffentlicht, 41 p. (in German).
- Schön J., 1983: *Petrophysik*. Ferdinand Enke Verlag, Stuttgart, 405 p.
- Schutz K. I., 1994: Structure and stratigraphy of the Gulf of Suez, Egypt (abs). *AAPG Bull.*, **81**, 8, 1411.
- Tramontini C., Davies D., 1969: A seismic refraction survey in the Red Sea. *Geophys. J. R. Astron. Soc.*, **17**, 2225–2241.